

How to Attain Communication-Efficient DNN Training? Convert, Compress, Correct

Zhong-Jing Chen¹, Eduin E. Hernandez², Yu-Chih Huang³, and Stefano Rini⁴

National Yang-Ming Chiao-Tung University (NYCU), Hsinchu City, Taiwan

{¹zhongjing.ee10, ²eduin.ee08, ³jerryhuang, ⁴stefano.rini}@nycu.edu.tw

Abstract—In this paper, we introduce CO₃, an algorithm for communication-efficiency federated Deep Neural Network (DNN) training. CO₃ takes its name from three processing applied steps which reduce the communication load when transmitting the local gradients from the remote users to the Parameter Server. Namely: (i) gradient quantization through floating-point conversion, (ii) lossless compression of the quantized gradient, and (iii) quantization error correction. We carefully design each of the steps above so as to minimize the loss in the distributed DNN training when the communication overhead is fixed. In particular, in the design of steps (i) and (ii), we adopt the assumption that DNN gradients are distributed according to a generalized normal distribution. This assumption is validated numerically in the paper. For step (iii), we utilize an error feedback with memory decay mechanism to correct the quantization error introduced in step (i). We argue that this coefficient, similarly to the learning rate, can be optimally tuned to improve convergence. The performance of CO₃ is validated through numerical simulations and is shown having better accuracy and improved stability at a reduced communication payload.

Index Terms—DNN training; Distributed optimization; Gradient compression; Lossless compression; Error feedback.

I. INTRODUCTION

As the size and complexity of modern-day Deep Neural Networks (DNN) are ever-increasing, high performance is attainable only by training the network over a tremendous amount of data. In this training regime, data centralization is no longer feasible for two main reasons: on one hand, the volume of data is too large to be communicated and stored centrally and, on the other hand, the centralization presents too many concerns from the robustness, privacy, and security standpoint. For the reasons above, distributed DNN training has received much attention in the recent literature, both from a distributed [1] parallel, [2] and networked computing perspective.

In this paper, we consider the distributed DNN training in which a centralized model is trained over datasets present at remote users. For this scenario, we propose CO₃, a novel joint training/communication scheme in which, at each iteration, the gradients at the remote users are first (i) converted to low-resolution floating point representations, then (ii) compressed losslessly, and then communicated to the Parameter Server (PS) through a finite-capacity link. At the next iteration, the remote users (iii) correct the quantization error by adding its scaled version to the current gradient before (i) is repeated

in the next iteration. Crucial in the design of CO₃ is the assumption that gradients can be well modelled as generalized normal (GenNorm) i.i.d. samples. This assumption is numerically validated in the paper for different DNN models and training regimes. In our simulation, we show that this approach provides excellent training performances at very low transmission rates between the remote user and the PS.

Relevant Literature: In recent years, distributed learning has received considerable attention in the literature [3]. Among various distributed optimization frameworks, federated learning (FL) has received particular attention in the recent literature [4]–[9]. FL consists of a central model which is trained locally at the remote clients by applying Stochastic Gradient Descent (SGD) over a local dataset. The local gradients are then communicated to the central PS for aggregation into a global model. A natural constraint in distributed and decentralized optimization is with respect to transmission rates between nodes and its relationship to the overall accuracy [10], [11]. Accordingly, one is interested in devising rate-limited communication schemes that attain high accuracy at a low overall communication payload. This can be attained through two steps: (i) dimensionality reduction, and (ii) quantization and compression. The dimensionality-reduction schemes put forth in the literature rely on various sparsification approaches [4], [6]. For instance, top_K is a rather aggressive sparsification method that keeps only the coordinates with the largest magnitudes [12], [13]. Dimensionality-reduction can also be performed on the whole gradient vector as suggested in [14] through an algorithm referred to as vector QSGD (VQSGD). In [15], the authors propose a choice of distortion which promotes sparse gradient quantization, conceptually generalizing top_K .

Following dimensionality reduction, the gradient can be digitized through quantization, either scalar-wise [15]–[17] or vector-wise [14]. From an implementation-oriented perspective, [18] studies the effect of gradient quantization when constrained to a *sign-exponent-mantissa* representation. After quantization, enabled by the statistical model obtained via extensive simulations that gradients in DNN training with SGD follows i.i.d. GenNorm, lossless compression can be applied to further reduce the communication rate toward the PS in a preliminary version of the present work [19].

When gradients are compressed, it has been shown that error

correction, or error feedback, can greatly improve performance [20]. Error feedback for 1-bit quantization was originally considered in [21]. In [22], error feedback is applied to gradient compression in a more general manner than [21].

Contributions: In this paper, we consider the problem of efficient gradient compression for rate-limited distributed DNN training. The main contributions of the paper can be found in the following two sections:

- a) **Sec. III – Validation of the GenNorm assumption:** A fundamental assumption of our algorithm design is the observation that the DNN gradient can be well approximated as a i.i.d. generalized normal samples. In Sec. III we numerically validate this assumption over a various DNN examples. It is worth emphasizing that through validating the GenNorm assumption, we are able to build an accurate statistical models for gradients in DNN training. This statistical model is of practical importance in its own right.
- b) **Sec. IV – Design of CO₃:** Using the GenNorm assumption as a stepping stone, we propose CO₃ as an efficient algorithm for the distributed training of DNN models over communication-constrained FL scenario.

Let us comment on these two sections in more details.

- a.i) **GenNorm modelling:** To the best of our knowledge, a good statistical model for modelling gradients in DNN training is currently lacking. We argue that one can effectively model such gradients as i.i.d. GenNorm variables. We also argue that the gradient distribution approaches the normal distribution as the depth of the network increases and as the epoch number increases. Additionally, we contend that the kurtosis of the gradient distribution provides a useful measure of the concentration of gradient around zero.
- a.ii) **Numerical validation:** We use statistical methods to validate the GenNorm assumption for three DNN architectures in the image classification task, namely DenseNet [23], ResNet [24], and NASNet [25], across both layers and training epochs.
- a.iii) **Error feedback:** In FL, error feedback is an effective mechanism to compensate the quantization error at the remote users. We argue, in Sec. IV-C, that the GenNorm assumption remains valid when error feedback is employed in distributed SGD.

Having numerically validated our assumption on the gradient distribution, we then move to the design of a communication-efficient algorithm for distributed DNN training. The proposed scheme, which we term CO₃, is comprised of the following three gradient processing steps:

- b.i) **Floating point (fp) conversion:** As a quantization mechanism, we consider fp conversion due its compatibility with gpu gradient processing. As in [18], we choose the exponent bias to minimize the L_2 loss between the original and quantized gradient.
- b.ii) **Lossless gradient compression:** Leveraging the GenNorm modeling of the local gradients, we further compress the quantized gradients using lossless compression in the form of Huffman coding.

- b.iii) **Error correction:** The quantization error is stored at one iteration and corrected in the next. We further employ a memory decay coefficient which prevents the accumulation of stale gradients.

Notation. Lowercase boldface letters (e.g., \mathbf{z}) are used for tensors, uppercase letters for random variables (e.g. X), and calligraphic uppercase for sets (e.g. \mathcal{A}). We also adopt the short-hands $[m : n] \triangleq \{m, \dots, n\}$ and $[n] \triangleq \{1, \dots, n\}$. Both subscripts and superscripts letters (e.g. g_t and $g^{(u)}$) indicate the iteration index and the user index for a tensor, respectively. Finally, \mathbb{F}_2 is the binary field. The all zero vector is indicated as $\mathbf{0}$.

II. SYSTEM MODEL

In many FL scenarios of practical relevance, the communication from the remote users and the PS is severely constrained in terms of transmission rate. For this reason, in the following, we consider the approach of [11], [15], [19] and investigate the accuracy/payload trade-off of distributed optimization. In Sec. II-E we specialized the general setting of [11], [19] to the specific case of federated DNN training.

A. Distributed Optimization

Consider the scenario with U remote users, each possessing a local dataset

$$\mathcal{D}^{(u)} = \left\{ \left(\mathbf{d}_k^{(u)}, v_k^{(u)} \right) \right\}_{k \in [|\mathcal{D}^{(u)}|]}, \quad (1)$$

where $\mathcal{D}^{(u)}$ includes $|\mathcal{D}^{(u)}|$ pairs, each comprising a data point $\mathbf{d}_k^{(u)}$ and the label $v_k^{(u)}$ for $u \in [U]$. Users collaborate with the PS to minimize the loss function \mathcal{L} as evaluated across all the local datasets and over the choice of the model $\mathbf{w} \in \mathbb{R}^d$, that is

$$\mathcal{L}(\mathbf{w}) = \frac{1}{|\mathcal{D}|} \sum_{u \in [U]} \sum_{k \in [|\mathcal{D}^{(u)}|]} \mathcal{L}(\mathbf{w}; \mathbf{d}_k^{(u)}, v_k^{(u)}). \quad (2)$$

For the *loss function* \mathcal{L} in the LHS of (2), we assume that there exists a unique minimizer \mathbf{w}^* . A common approach for numerically determining this unique minimizer, \mathbf{w}^* , is through the iterative application of (synchronous) stochastic gradient descent (SGD). In the SGD algorithm, the model parameter \mathbf{w} is updated at each iteration t , by taking a step toward the negative direction of the stochastic gradient vector, that is

$$\mathbf{w}_{t+1} = \mathbf{w}_t - \eta_t \mathbf{g}_t, \quad (3)$$

for $t \in [T]$, a choice of initial model \mathbf{w}_0 , and where \mathbf{g}_t is the stochastic gradient of $\mathcal{L}(\cdot)$ evaluated in \mathbf{w}_t , that is $\mathbb{E}[\mathbf{g}_t] = \nabla \mathcal{L}(\mathbf{w}_t)$. Finally, η_t in (3) is an iteration-dependent step size, called *learning rate*.

In the FL setting, the SGD iterations are distributed among U users and is orchestrated by PS as follows: (i) each user $u \in [U]$ receives the current model estimate, \mathbf{w}_t of the optimal model \mathbf{w}^* over the infinite capacity link from the PS. The user $u \in [U]$ then (ii) accesses its local dataset $\mathcal{D}^{(u)}$ and computes the local stochastic gradient $\mathbf{g}_t^{(u)}$. Finally (iii) each

node communicates the gradient estimate $\mathbf{g}_t^{(u)}$ to the PS which then computes the term \mathbf{g}_t as

$$\mathbf{g}_t = \frac{1}{U} \sum_{u \in [U]} \mathbf{g}_t^{(u)}, \quad (4)$$

and uses \mathbf{g}_t to update the model estimate.

B. Rate-limited distributed training

In the rate-limited distributed training scenario [11], [15], [19], communication between each user and the PS takes place over a noiseless channel with finite capacity. On the other hand, communication between the PS and remote users is unconstrained.

A general three-step scheme to address the finite transmission rate between remote users and PS is described as follows.

(i) Pre-processing: Assume that at time t the local gradient $\mathbf{g}_t^{(u)}$ becomes available at the remote user u . This value is fed into a function $f : \mathbb{R}^d \rightarrow \mathbb{R}^d$ to form $\mathbf{v}_t^{(u)} = f(\mathbf{g}_1^{(u)}, \dots, \mathbf{g}_t^{(u)})$. Here, the function f is introduced to allow pre-processing before quantization. In our work, f is meant to as a correction mechanism for quantization error introduced next. We note that when $f(\mathbf{x}) = \mathbf{x}$, i.e., the identity function, the above procedure reduces to simply quantization as in [11], [19].

(ii) Quantization: the term $\mathbf{v}_t^{(u)}$ is quantized via a quantizer $Q : \mathbb{R} \rightarrow \mathcal{X}$ to form the representative $\hat{\mathbf{v}}_t^{(u)} = Q(\mathbf{v}_t^{(u)})$, where \mathcal{X} is the collection of representatives, i.e., quantization levels. The mapping Q is meant as a stochastic mapping, so that non-subtractive dither quantization can be implemented.

(iii) Lossless compression: Following quantization, the quantized gradients are further compressed through the mapping $h : \mathcal{X} \rightarrow \mathbb{F}_2^*$ to form a codeword $\mathbf{b}_t^{(u)} = h(\hat{\mathbf{v}}_t^{(u)})$. Here, we allow h to be a variable-length coding scheme; hence, the range is \mathbb{F}_2^* , where \mathbb{F}_2 is the binary field. This compression step is lossless, that is, the mapping h is invertible: The role of this mapping is to remove the statistical redundancy inherent in the local gradients, thus reducing the amount of bits to be transmitted to the PS. Finally, let $r_t^{(u)}$ be the length of $\mathbf{b}_t^{(u)}$.

At the PS, the gradient of user $u \in [U]$ at time t is reconstructed $\hat{\mathbf{g}}_t^{(u)}$ and the model is updated as

$$\hat{\mathbf{w}}_t = \hat{\mathbf{w}}_{t-1} + \frac{\eta t}{U} \sum_{u \in [U]} \hat{\mathbf{g}}_t^{(u)}. \quad (5)$$

The above steps are repeated for all $t \in [T]$. At time $t = T$ the model $\hat{\mathbf{w}}_T$ is declared as the approximate value of \mathbf{w}^* .

C. Gradient assumptions

A meaningful engineering approach to the design of the steps in Sec.II-B can be established only under some regularity assumption on the value of the local gradients. In this paper we shall adopt the following assumption: Let us assume that the local gradients are distributed i.i.d. according to \mathbb{P}_{G_t} at each user, that is $\mathbf{g}_t^{(u)} \sim \mathbb{P}_{G_t}$ is i.i.d for all $u \in [U]$.

With respect to the i.i.d. assumption, we notice that mean field theory has provided a partial validation of this assumption. In series of extremely interesting papers [26]–[29], it

has been shown that, in various regimes, DNN weights in a given layer become indistinguishable as the number of SGD steps grow large. For instance, [27] considers a DNN with a fixed number of layers and any width trained to minimize the square loss over an i.i.d. dataset. In this scenario, the authors show that training through SGD is well-approximated by continuous dynamics expressed through certain non-linear partial differential equation. As a result of this approximation, the weights can be well-approximated through *distributional dynamics* [30] which shows that the per-layer DNN weights are indistinguishable. Note that the analysis of SGD dynamics for DNNs has been developed that connects naturally to the theory of universal approximation [31].

D. Problem formulation

Under the assumption that a gradient distribution can be properly defined, we can then define the expectation of the performance of a scheme in the framework of Sec. II-B. Remembering that $r_t^{(u)}$ is the length of $\mathbf{b}_t^{(u)}$, the transmitted binary string, we define the expected length of $u \in [U]$ at $t \in [T]$ as

$$R_t^{(u)} = \mathbb{E}_{f, Q, h} [r_t^{(u)}], \quad (6)$$

where the expectation is taken w.r.t. the product gradient distribution until time t , $\prod_{t' \in [t]} \mathbb{P}_{G_{t'}}$. The *communication overhead* of a certain choice of functions (f, Q, h) as the sum expected lengths conveyed over the up-link channel over the training, that is

$$R = \sum_{t \in [T]} \sum_{u \in [U]} R_t^{(u)}. \quad (7)$$

Using the definition in (7), we finally come to the definition of the accuracy/overhead trade-off for as

$$L_T(R) = \min_{f, Q, h} \mathbb{E} [\mathcal{L}(\mathbf{w}_T)], \quad (8)$$

where the expected value is over the stochasticity in the gradient evaluation and the distribution of the gradients. In other words, $L_T(R)$ is the minimum loss that one can attain in T iterations when the total communication payload is R . Note that the minimization is over the pre-processing, quantization, and lossless compression operations.

E. DNN training

While we have so far considered a general distributed optimization problem, in the remainder of the paper we shall consider the particular case of DNN training. More specifically, we consider the training for the CIFAR-10 dataset classification task using the following three architectures: (i) DenseNet121, (ii) ResNet50V2, and (iii) NASNetMobile. For each architecture, the training is performed using SGD optimizer with a constant $\eta = 0.01$ learning rate in (5). The rest of the configurations of the parameters and hyperparameters used for the training are specified in Tab. I.

During each batch-iterations, the gradients of the trainable parameters are accumulated on a temporal memory on a per layer basis with the intention on averaging them along the

TABLE I: Parameters and hyperparameters used for the training of the DNN models.

Dataset	CIFAR-10
Training Samples	5.00×10^4
Test Samples	1.00×10^4
Optimizer	SGD
Learning Rate	1×10^{-2}
Momentum	0
Loss	Categorical Cross Entropy
Epochs	150
Mini-Batch Sizes	64

TABLE II: Total number of layers, weight parameters, and trainable weight parameters belonging to each architecture.

Architectures	Layers	Total Params	Train Params
DenseNet121	121	7.05×10^6	6.96×10^6
ResNet50V2	50	2.36×10^7	2.35×10^7
NASNetMobile	-	4.28×10^6	4.24×10^6

epoch. At the end of the epoch, the gradients are saved and the temporal memory is freed. This process is repeated until the last epoch for the gradient analysis provided in the next subsections.¹ As these are very deep networks as specified in Tab. II, we will limit the scope to three layers in each of the architectures: one 2-dimensional convolution layer located in the upper, middle, and lower sections of the networks. Tab. III details the number of trainable weight parameters for these chosen layers.

F. Further comments

Before delving further in the paper, let us add a few brief comments on some aspects of the problem formulation in Sec. II-D which are not considered in the paper.

Asynchronous/delayed gradients: In the paper, we only consider the case in which training occurs *simultaneously and synchronously* at all remote users. This is an idealized assumption which rarely holds in practical scenarios. Although asynchronous training and delayed gradients are a very pressing and interesting problem, it is not considered in the following.

Across-layer correlation. In the following we compress the gradients distribution as independent across iterations. Although correlation of the gradients across layers exist, we do not consider such correlation. For instance, in [27], it is shown that the per-layer distribution is conditionally dependent only on the weights in the previous layer. For simplicity, in the following we do not consider this dependency. The design of

¹The code for the gradient modeling and analysis is available at https://github.com/Chen-Zhong-Jing/CO3_algorithm

TABLE III: Number of trainable weight parameters for the chosen layers of each architecture.

Architectures	Upper	Middle	Lower
ResNet50V2	4.10×10^3	3.28×10^4	5.24×10^5
DenseNet121	9.41×10^3	1.64×10^4	6.55×10^4
NASNetMobile	3.87×10^3	3.10×10^4	1.86×10^5

a version of the proposed approach taking advantage of this correlation is left for future research.

Lossless compression: In this paper, we consider the *lossless compression* scenarios in which the PS is interested in the exact reconstruction of the quantized gradients $\hat{\mathbf{v}}_t^{(u)}$ from $\mathbf{b}_t^{(u)}$. Our choice is generally dictated by the fact that a precise understanding of the effect of the distortion criteria used for compression on the learning performance is unclear. For instance, top_K sparsification [32] suggests that an appropriate choice of distortion should take into account the gradient magnitude. This is in contrast with the compression error introduced by the classic mean squared error (MSE) criteria which is commonly used in practical lossless compression algorithms. The authors of [15] consider a weighted norm approach which bridges the compression through top_K and that of MSE criteria. The intuition between this choice distortion is the fact that the gradient with larger magnitude are more relevant to the DNN training.

Universal compression: In the paper we consider distribution-based compression. When the underlying gradient distribution is unknown, one can employ Lempel-Ziv coding [33], which is asymptotically optimal in terms of the expected length, even when the gradient are generated by a rather general (and yet unknown) source [34]. Despite of such wide applicability, the performance of such an universal source coding scheme is generally not acceptable in the short to medium source length regime. In contrast, in the presence of knowledge about $\mathbb{P}_{\tilde{G}_t}$, optimal lossless compression can be easily achieved by Huffman coding [35]. Additionally, universal approaches have a generally higher implementation complexity and memory occupation which might not be amenable to low-cost and fast implementation.

III. GRADIENT MODELLING FOR DNN GRADIENTS

As a first contribution of the paper, we wish to argue that the DNN gradient distribution \mathbb{P}_{G_t} , if exists, can be well modelled, in each layer, as an i.i.d. GenNorm distribution. The GenNorm parameters are assumed to change across layer and across iteration but all variables are otherwise independent.

In its parametrization through a location, scale, and shape parameter – μ , α , and β respectively, the pdf of the GenNorm distribution is obtained as

$$X \sim \text{GenNorm}(x, \mu, \alpha, \beta) \implies f_X(x) = \frac{\beta}{2\alpha\Gamma(1/\beta)} \exp\left\{-\left(\frac{|x-\mu|}{\alpha}\right)^\beta\right\}, \quad (9)$$

The mean, variance, and kurtosis of $X \sim \text{GenNorm}(x, \mu, \alpha, \beta)$ have the following expressions:

$$\text{Mean}(X) = \mu \quad (10a)$$

$$\text{Var}(X) = \frac{\alpha^2\Gamma(3/\beta)}{\Gamma(1/\beta)} \quad (10b)$$

$$\text{Kurt}(X) = \frac{\Gamma(5/\beta)\Gamma(1/\beta)}{\Gamma(3/\beta)^2}. \quad (10c)$$

GenNorm is a family of distributions that subsumes Laplace ($\beta = 1$) and Normal ($\beta = 2$) distributions as special

cases. When the shape parameter $\beta < 2$, the distribution is leptokurtic and has a heavier tail than the normal distribution.

With the consideration above, we now state the working assumption that shall guide the design of the proposed scheme, CO₃, in Sec. IV.

Assumption. GenNorm DNN gradients: *For each layer and for each epoch, the DNN gradients are distributed according to the GenNorm distribution in (9).*

For brevity, we refer to the above assumption as the GenNorm assumption. With respect to the validity of the of the GenNorm assumption, we notice that recently the authors of [36] have argued that gradients possess a Laplace distribution, partially supporting our assumption.

In the remainder of the section, we shall motivate the GenNorm assumption from a statistical perspective and further describe the dependency of the parameters on the layer depth and iteration number.

Remark (Error-Feedback). *In this section we shall consider the case in which no gradient pre-processing is performed, that is $f(\mathbf{x}) = \mathbf{x}$. In CO₃ we will consider the case in which f is an error feedback mechanism similar to that in [6]. In other words, the quantization error is accumulated and added as a correction term when quantizing the gradient in the new iteration. In order to improve the flow of the paper, the validation of the GenNorm assumption with error feedback is presented in Sec. IV-C.*

A. Statistical Validation

Let us begin by visually inspecting the gradient histogram for the networks in Sec. II-E, as depicted in Fig. 1. In this figure, we plot (i) the sample distribution, (ii) the GenNorm fitting, and (iii) the normal distribution (Norm) fitting for ResNet50V2 and NASNetMobile across three epoch: 2, 50, and 100. We observe that in the earlier epochs, the gradient histogram is closer to the GenNorm distribution in that the sample distribution is (i) more concentrated in zero, and (ii) it contains heavier tails than the Norm distribution. As the training continues, the variance of the gradient distribution gradually reduces and approaches the Norm distribution. For instance, the gradients from ResNet50V2 seem to converge to the Norm distribution slower than NASNetMobile.

Fig. 1 only provides a qualitative depiction of the GenNorm assumption. A quantitative depiction is provided in Fig. 2 and 3, where we plot the 1D W_2 Wasserstein distance [37], defined as

$$W_2(X, Y) = \left(\int_0^1 |F_X^{-1}(z) - F_Y^{-1}(z)| dz \right)^{1/2}, \quad (11)$$

between (i) GenNorm distribution and the gradient samples, (ii) the Norm distribution and the gradient samples, and the Laplace distribution and the gradient samples for the upper layer DenseNet121 and NasNetMobile as a function of the epoch number. Note that Wasserstein distance is a distance metric measuring the distance between two probability distributions and is recently very popular for many machine learning applications due to its many nice properties. From Fig. 2, both

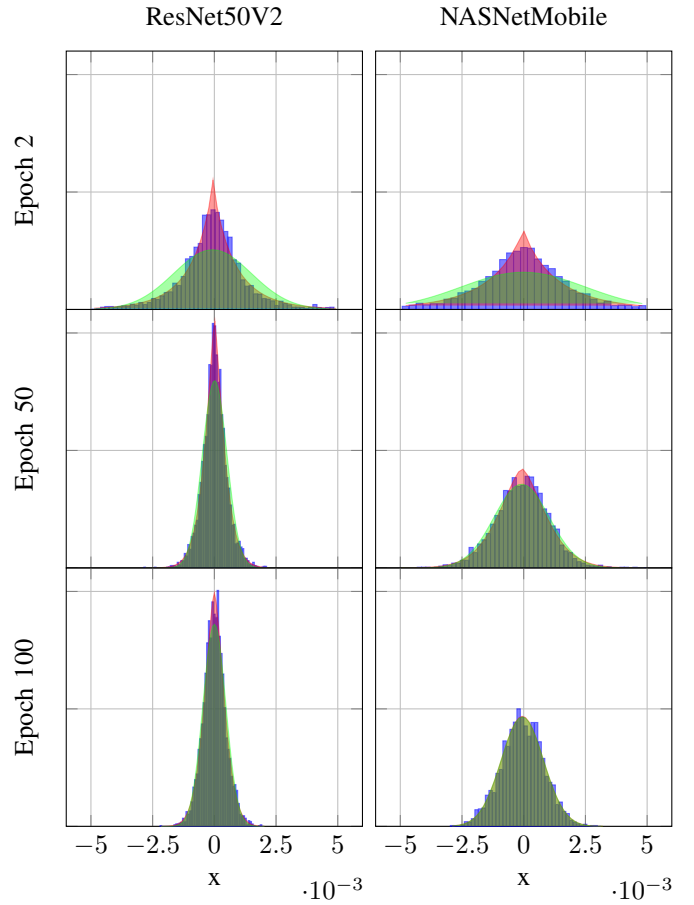


Fig. 1: Histogram of gradient (blue) with PDF of GenNorm (red) and Norm (green) of top layer for epoch 2, 50, and 100 in two different network.

Laplace and GenNorm distribution provide a closer fitting with gradient samples than the Norm, with GenNorm providing the lowest loss. Notice that Laplace and Norm distribution maintain a constant separation between their errors in comparison to GenNorm since the first two only require optimization of the scale parameter, α , in comparison to GenNorm which is also requires tuning of β . From Fig. 3, the Laplace distribution is outperformed by the Norm after the first few epochs, but GenNorm still maintains the advantage, showing its flexibility in adapting the tails to better fit the distribution. Additionally, for both Figs. 2, 3 we notice the relative distance between GenNorm and Norm decreases with the epoch number, again suggesting that for large enough epoch number the gradient distribution tends towards the Norm.

B. Distribution parameters

The mean and variance of the sample gradient distribution is provided in Table. IV, together with the respective confidence interval. Another important aspects of the GenNorm is that it highlights the role of the kurtosis in describing the behaviour of the gradients, as in (10c), the kurtosis depends only on the parameter β . In Figs. 4 and 5, we plot the excess kurtosis (i.e., the kurtosis minus 3). Observation of the excess kurtosis

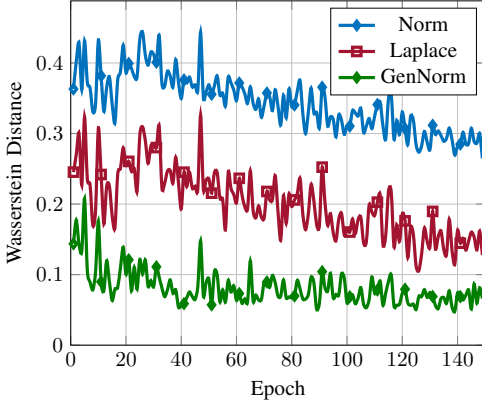


Fig. 2: W_2 distance between the empirical CDF and best-fit CDF for gradient in upper layer of DenseNet121 for various gradient assumptions.

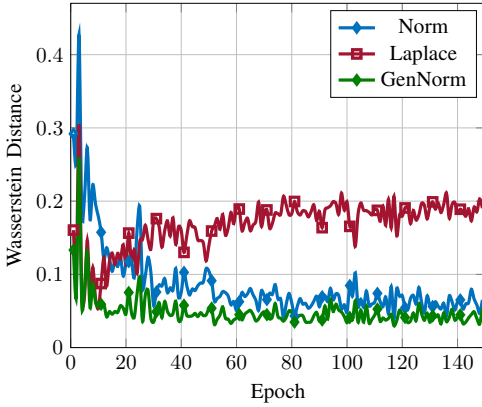


Fig. 3: W_2 distance between the empirical CDF and best-fit CDF for gradient in upper layer of NASNetMobile for various gradient assumptions.

for the upper layers in Fig. 4 and in Fig. 5 provides us further insight on previous behaviour from Figs. 2, 3: for DenseNet121, the excess kurtosis suggests the distribution requires longer tails than Norm while for the NasNetMobile later epochs suggests the excess kurtosis approximates the Norm distribution, hence why Laplace had a lower loss than Norm in Fig. 2 and why the opposite happened in Fig. 3. Results in these figures again indicate the GenNorm modeling tending towards the Norm with further epochs (excess kurtosis evolving from positive to near 0).

IV. PROPOSED APPROACH: CO_3

In this section, we propose a novel algorithm for communication-efficient distributed DNN training, named CO_3 . This algorithm implements the operations in Sec. II-B: (i) pre-processing is error correcting with a memory decay, that is f that accumulates a version of the quantization error of the previous epoch; (ii) quantization is chosen as fp conversion, optimized over the exponent bias. Finally, compression is Huffman coding using the GenNorm assumption over the quantized gradients. In Sec. IV-A, we introduce the algorithm in its general form. In Sec. IV-B, we specialize the proposed

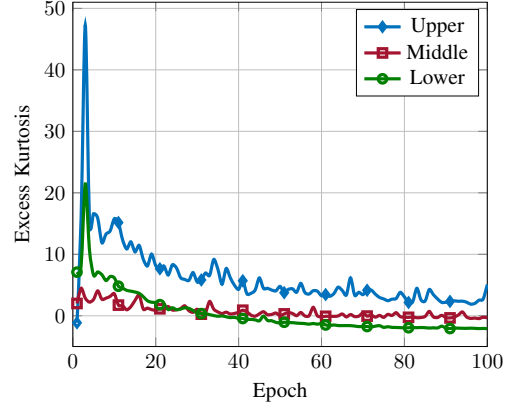


Fig. 4: DenseNet121: Excess kurtosis of the gradients of the upper, middle, and lower convolution layer.

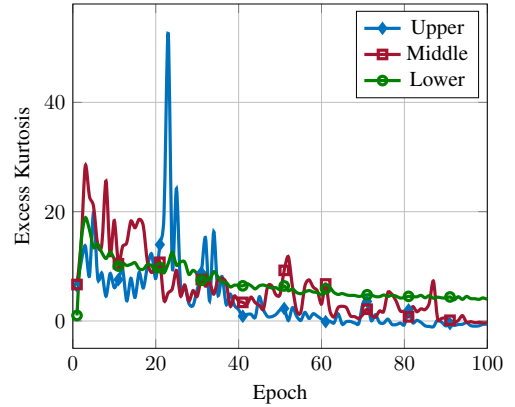


Fig. 5: NASNetMobile: Excess kurtosis of each convolution layer.

CO_3 to DNN models and detail the operations in the proposed algorithm. Since the algorithm requires knowledge of the underlying distribution of quantization outputs, in Sec. IV-C, we return to the approach in Sec. III and argue that the GenNorm assumption is again valid even in the presence of error feedback. Finally, in Sec. IV-D, we investigate the magnitude of the error term and that of the gradient during the learning process to determine the weighting of the memory in the proposed CO_3 algorithm.

A. CO_3 algorithm

In the following, we propose a novel algorithm, named CO_3 , which falls within the general framework described in Sec. II-B. More precisely, CO_3 considers the following gradient processing steps (i) the quantization, Q , is chosen as the fp conversion, (ii) compression, h , is chosen as element-wise Huffman coding, and (iii) an f that performs error correction with a memory decay of γ .

Next, let us describe each of the steps above in further detail:

(i) fp conversion: the local gradient $\mathbf{g}_t^{(u)}$ is converted into the fp representation $[\text{sgn}, \text{mant}, \text{exp}]$ with $\text{sgn} = 1$ bit for the sign, mant bits for the mantissa and exp bits for the exponent. Furthermore, at each time t , we introduce a bias b_t on the

TABLE IV: The mean and variance of NASNetMobile’s gradient at different epochs

Layers		Epoch 2	Epoch 50	Epoch 100
Upper	mean	$-1.72 \times 10^{-5} \pm 1.12 \times 10^{-7}$	$-8.38 \times 10^{-5} \pm 1.90 \times 10^{-8}$	$-5.53 \times 10^{-5} \pm 2.13 \times 10^{-8}$
	variance	$9.58 \times 10^{-5} \pm 8.03 \times 10^{-8}$	$1.86 \times 10^{-5} \pm 3.82 \times 10^{-10}$	$1.07 \times 10^{-5} \pm 1.82 \times 10^{-11}$
Middle	mean	$6.66 \times 10^{-6} \pm 9.53 \times 10^{-9}$	$1.10 \times 10^{-5} \pm 8.57 \times 10^{-9}$	$3.68 \times 10^{-6} \pm 1.92 \times 10^{-9}$
	variance	$4.96 \times 10^{-6} \pm 1.19 \times 10^{-10}$	$3.56 \times 10^{-6} \pm 7.66 \times 10^{-11}$	$1.93 \times 10^{-6} \pm 7.31 \times 10^{-13}$
Lower	mean	$8.97 \times 10^{-5} \pm 4.40 \times 10^{-9}$	$4.85 \times 10^{-6} \pm 3.88 \times 10^{-10}$	$5.10 \times 10^{-7} \pm 3.13 \times 10^{-11}$
	variance	$4.74 \times 10^{-7} \pm 4.99 \times 10^{-14}$	$2.24 \times 10^{-7} \pm 2.52 \times 10^{-15}$	$1.96 \times 10^{-7} \pm 6.30 \times 10^{-16}$

exponent so as to minimize the expected loss between the closest quantization representative and $\mathbf{g}_t^{(u)}$, that is

$$b_t = \underset{b}{\operatorname{argmin}} \mathbb{E} \left[|c_{\text{sgn}} \cdot c_{\text{mant}} \cdot 2^{c_{\text{exp}}+b} - G_t|^2 \right], \quad (12)$$

where $b \in \mathbb{R}$ and the expectation is over the gradient distribution $\mathbb{P}_{\mathbf{G}_t}$. A more principled approach to gradient quantization can be considered; see [15] for example. Here, we focus on fp conversion as it can be implemented with extreme computational efficiency.

Let us denote the fp quantization strategy as $Q_{\text{fp}}(\cdot)$ in the following.

(ii) Huffman coding: After fp conversion, the quantized gradient $\widehat{\mathbf{g}}_t^{(u)}$ is compressed using Huffman coding. As Huffman coding requires the distribution of data sources, we assume that the underlying distribution is GenNorm. Note that this assumption has been validated in Section III for distributed DNN training without error correction. In Section IV-C, we will verify this assumption again through simulations and obtain the corresponding parameters for distributed DNN with error feedback. A different code is used in each DNN layer, but the same code is used across all users at a given layer. Note that, as for the fp conversion, the Huffman coding is chosen for CO₃ as it can be implemented with minimum requirements for both computation and memory. This is in contrast to other universal compression algorithms, such as LZ74 [33], which do not rely on any assumption on the source distribution. A comparison in terms of gradient compression ratio between these two algorithms will be shown in Section V.

In the following, we indicate the Huffman lossless compression as $h_{\text{Hf}}(\cdot)$.

(iii) Error correction: Motivated by the success of error feedback in accelerating the convergence of models using compressed gradients [22], [38], we adopt a f in Sec. II-B that accumulates the quantization error from the previous epoch in the proposed CO₃. More precisely, for each $u \in [U]$ and a fixed $\gamma > 0$, we let

$$f(\mathbf{g}_1^{(u)}, \dots, \mathbf{g}_t^{(u)}) = \mathbf{g}_t^{(u)} + \gamma \mathbf{m}_{t-1}^{(u)}, \quad (13)$$

where $\mathbf{m}_0^{(u)} = \mathbf{0}$ and

$$\mathbf{m}_t^{(u)} = \gamma \mathbf{m}_{t-1}^{(u)} + \mathbf{g}_t^{(u)} - \widehat{\mathbf{g}}_t^{(u)}, \quad (14)$$

with $\widehat{\mathbf{g}}_t^{(u)} = Q_{\text{fp}}(f(\mathbf{g}_1^{(u)}, \dots, \mathbf{g}_t^{(u)}))$ being the quantization output. It is worth mentioning that (13) depends on $\mathbf{g}_1^{(u)}, \dots, \mathbf{g}_{t-1}^{(u)}$ only through $\mathbf{m}_{t-1}^{(u)}$; therefore, the algorithm can be easily implemented with limited memory resources. The parameter γ , which we refer to as *memory decay coefficient*, is used to discount the error accumulation and our

TABLE V: Recap of key parameters in alphabetical order.

Exponent Size	exp
Exponent Bias	b
fp Quantization	$Q_{\text{fp}}(\cdot)$
Gradient	\mathbf{g}
Huffman Lossless Compression	$h_{\text{Hf}}(\cdot)$
Learning Rate	η
Mantissa Size	mant
Memory	\mathbf{m}
Memory Decay Coefficient	γ
Sign	sgn
Total Time	T
Total Users	U

numerical experiments in Section IV-C will show that a judicious choice of γ is crucial in tuning performance.

We summarize the proposed CO₃ in Algorithm 1, where Line 2 is to initialize $\mathbf{m}_0^{(u)}$; Line 8 first adds a version of quantization error from the previous epoch to the local gradient and performs quantization; Line 9 further compresses the output via a Huffman code; and Line 10 computes the quantization error of the current epoch. A summary of the parameters in the proposed approach is provided in Table. V.

Algorithm 1 Proposed Algorithm: CO₃

Require: Local datasets $\{\mathcal{D}_u\}_{u \in [U]}$, loss function $\mathcal{L}(\cdot)$, initial model estimate $\widehat{\mathbf{w}}_0$

Require: learning parameter η , memory decay parameter γ

```

1: for  $u \in [U]$  do
2:   user  $u$  sets memory to zero  $\mathbf{m}_0^{(u)} = \mathbf{0}$ 
3: end for
4: for  $t \in [T]$  do
5:   PS sends  $\widehat{\mathbf{w}}_t$  to all remote users
6:   for  $u \in [U]$  do
7:     user  $u$  evaluates the local gradient  $\mathbf{g}_t^{(u)}$ 
8:     user  $u$  fp-converts  $\mathbf{g}_t^{(u)}$ :  $\widehat{\mathbf{g}}_t^{(u)} = Q_{\text{fp}}(\mathbf{g}_t^{(u)} + \gamma \mathbf{m}_{t-1}^{(u)})$ 
9:     user  $u$  compresses  $\widehat{\mathbf{g}}_t^{(u)}$ :  $\mathbf{b}_t^{(u)} = h_{\text{Hf}}(\widehat{\mathbf{g}}_t^{(u)})$ 
10:    user  $u$  updates  $\mathbf{m}_t^{(u)} = \gamma \mathbf{m}_{t-1}^{(u)} + \mathbf{g}_t^{(u)} - \widehat{\mathbf{g}}_t^{(u)}$ 
11:    user  $u$  sends  $\mathbf{b}_t^{(u)}$  to the PS
12:   end for
13:   PS decompresses all the users gradients as  $\{\widehat{\mathbf{g}}_t^{(u)}\}_{u \in [U]}$ 
14:   PS updates the model as  $\widehat{\mathbf{w}}_{t+1} = \widehat{\mathbf{w}}_t + \frac{\eta}{U} \sum_{u \in [U]} \widehat{\mathbf{g}}_t^{(u)}$ 
15: end for
16: return  $\widehat{\mathbf{w}}_{T+1}$  an estimate of the optimal model  $\mathbf{w}^*$ 

```

Remark (Inconsequential number of users). *Note that in the approach of Algorithm 1, the number of remote users U does not influence the accuracy/payload tradeoff in (8). This is because the algorithm parameters are not chosen as a function*

of U . In actuality, one would indeed design these hyper-parameters as a function of the number of remote users.

Given the remark above, we suppress the superscript (u) from this point onward, due to the fact that the user index is inconsequential.

B. CO₃ for DNN

We now specialize the proposed CO₃ to DNN models. For our numerical evaluations, we consider the CIFAR-10 dataset classification task using the following three architectures: (i) DenseNet121, (ii) ResNet50V2, and (iii) NASNetMobile.² For each architecture, the training is performed using SGD optimizer with a constant $\eta_t = 0.01$ learning rate. The rest of the configurations of the parameters and hyper-parameters used for the training are specified in Tab. I.

Let us begin by revisiting the fp exponent bias in (12). Two $Q_{\text{fp}}(\cdot)$ are considered, namely $[\text{sgn}, \text{mant}, \text{exp}] = [1, 2, 1]$ and $[\text{sgn}, \text{mant}, \text{exp}] = [1, 5, 2]$, which we refer to as fp4 and fp8, respectively, in the sequel. For each $Q_{\text{fp}}(\cdot)$, we note that solving (12) explicitly is not easy at all due to the complicated nature of GenNorm distribution (which is evident by the fact that the rate-distortion problem remains unsolved for most β [39]) and that of the fp quantizers.

Here, we instead solve (12) via Monte-Carlo simulations for some isolated instances of β and then look for a polynomial to fit these simulated results. As a result, we are able to argue that, when the GenNorm assumption holds, then

$$b_t \approx (0.46 - 2.85\beta + 5.37\beta^2 - 2.85\beta^3 + 0.52\beta^4) / \sigma, \quad (15)$$

where β is the GenNorm shape parameter corresponding to the given DNN layer and σ^2 is the variance. In other words, b_t can be well-approximated with a polynomial that depends only on the shape parameter, once normalized by the variance. In the top of Fig. 6, we plot the numerically optimized b_t for fp4 as a function of β together with the approximation in (15) for the case in which the variance is unitary.

Similar tests are done for fp8 for which we obtain

$$b_t \approx (-5793 + 35605.5\beta - 76511.8\beta^2 + 68153\beta^3 - 18520.3\beta^4) / \sigma. \quad (16)$$

Moreover, the numerically optimized b_t for fp8 and the approximation in (16) are shown in the bottom of Fig. 6. In all of the following simulations, we will use (15) and (16) to select b_t for fp4 and fp8, respectively.

C. Validation of GenNorm assumption with error feedback

Next, we wish to validate the GenNorm assumption of Section III even when error correction is employed, that is when $\mathbf{g}_t + \gamma \mathbf{m}_{t-1}^{(u)}$ is considered. In Figs. 7 and 8, we plot the 1D W_2 Wasserstein distance between the sample empirical CDF and the best-fit CDF with $\gamma = 0.9$ and 0.7 , respectively, for the three families: (i) Norm, (ii) Laplace, and (iii) GenNorm distribution.

²We note that our following discussions are valid for all these three networks. However, to avoid repeating ourselves too many times, only a subset of the results is presented.

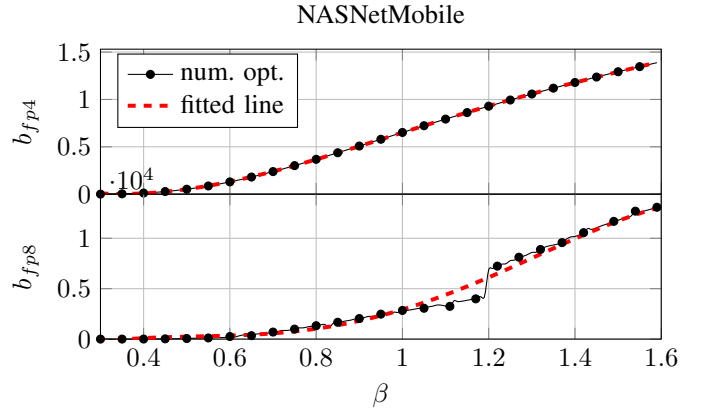


Fig. 6: The relation between β and b which minimizes the L_2 loss for fp4 and fp8 quantization.

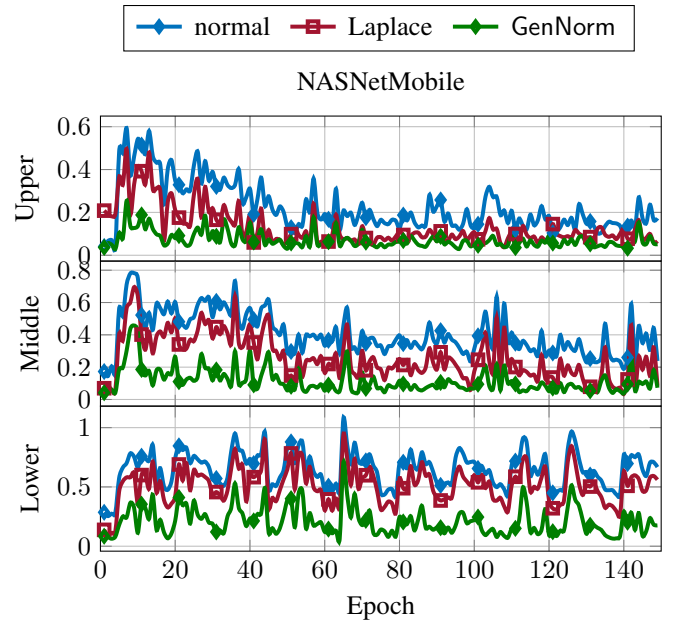


Fig. 7: W_2 distance between the empirical CDF and best-fit CDF for the term $\mathbf{g}_t + 0.9\mathbf{m}_{t-1}^{(u)}$ for each layer of NASNet-Mobile fp4 training.

From these two figures, we note that even accounting for the fact that GenNorm encompasses Norm and Laplace as special cases, the GenNorm distribution offers a much improved fitting of the empirical distribution of the samples to be quantized.

In Fig. 9, we repeat the simulation in Fig. 8 but replace fp4 with fp8. In this figure, one again observes that among the three families of distributions, GenNorm best matches the empirical distribution.

D. Error magnitude

Next, in Figs. 10 and 11, we investigate the magnitude of the memory term, \mathbf{m}_t , versus the gradient term, \mathbf{g}_t , in the error feedback mechanisms with $\gamma = 0.9$ and 0.7 , respectively. Note that the choice of magnitude as a performance metric has been justified in [20]. Here, for numerical stability, we change the

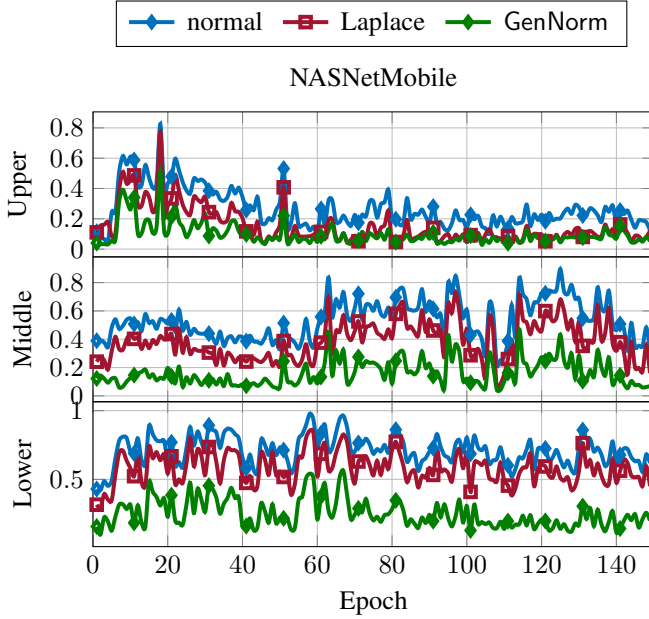


Fig. 8: W_2 distance between the empirical CDF and best-fit CDF for the term $\mathbf{g}_t + 0.7\mathbf{m}_{t-1}^{(u)}$ for each layer of NASNet-Mobile fp4 training..

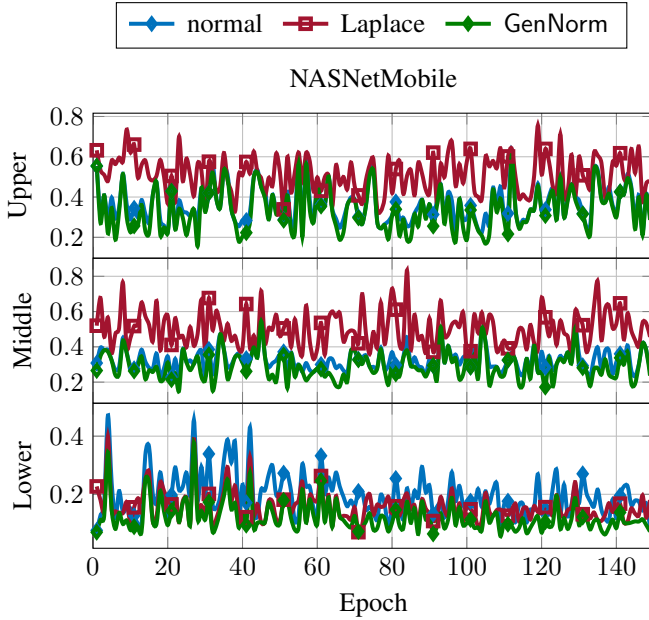


Fig. 9: W_2 distance between the empirical CDF and best-fit CDF for the term $\mathbf{g}_t + 0.7\mathbf{m}_{t-1}^{(u)}$ for each layer of NASNet-Mobile fp8 training.

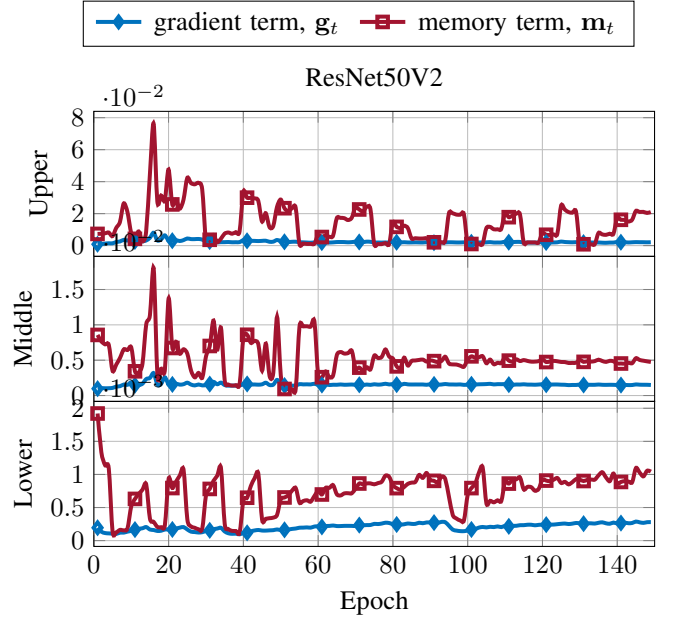


Fig. 10: L_1 norm of gradient and error term for upper, middle, and lower layers from the ResNet50V2 when $\gamma = 0.9$.

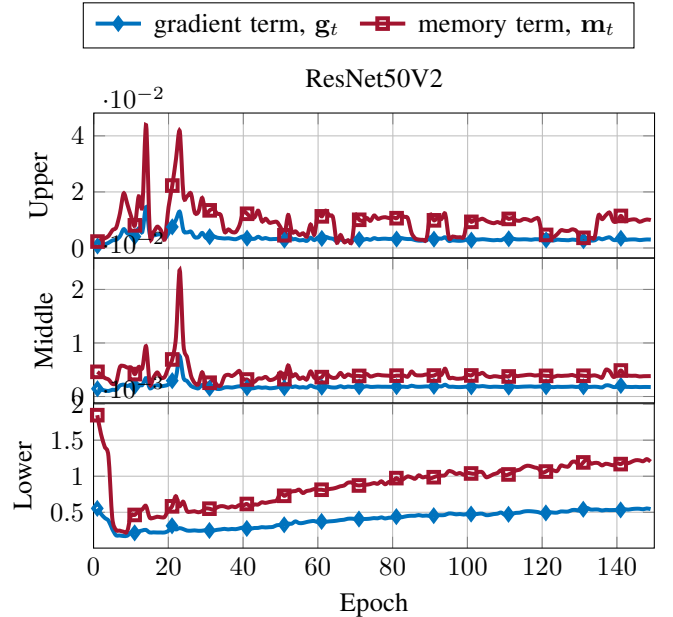


Fig. 11: L_1 norm of gradient and error term for upper, middle, and lower layers from the ResNet50V2 when $\gamma = 0.7$.

scale b_t only every 5 epochs and use the same b_t for the next 5 epochs. Now, we clarify various aspects of CO_3 . We begin by clarifying the simulation settings and then revisit the three main ingredients of CO_3 from a numerical point of view.

We note that the differences between the magnitudes of \mathbf{m}_t and \mathbf{g}_t in these two figures are quite stable for this choice of γ . By comparing these two figures and our results for other γ (not shown to avoid repetition), we conclude that $\gamma = 0.7$ is a fairly good choice that leads to a very stable and small difference between the magnitudes of \mathbf{m}_t and \mathbf{g}_t .

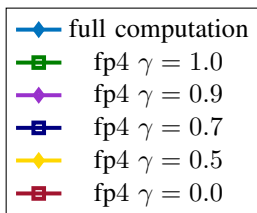


Fig. 12: Shared legend for Figs.13, 14, and 15

V. SIMULATION

We conclude the paper with some plots regarding the overall performance of the proposed CO_3 . The parameters are as shown in Tables I and II.

In Fig. 13, we plot the test accuracy against the epoch for the ResNet50V2. We consider the fp4 quantization with $[\text{sgn mant exp}] = [1, 2, 1]$ and various values of γ . Through our experimentation, we observe that as predicted in our results in Sec. IV-D, with $\gamma = 0.7$, the proposed CO_3 can provide a reasonably good accuracy performance that is comparable to the full SGD computation, while requiring $R_{fp4,Res} = 1.23 \times 10^2$ bits, a significantly less communication resource. Note that for $\gamma = 0$, it is essentially not using error feedback while $\gamma = 1$ is using a non-decaying error feedback. We repeat the simulation for NASNetMobile in Fig. 14, which shows similar results that with $R_{fp4,NAS} = 3.43 \times 10^{11}$ bits, the proposed CO_3 with $\gamma = 0.9$ is able to achieve the accuracy performance that is comparable to the full SGD computation. We note that the choice $\gamma = 0.9$ can also be justified by looking into our results for error magnitudes (not shown to save space). Moreover, similar results for fp8 with $[\text{sgn mant exp}] = [1, 5, 2]$ are presented in Fig. 15, where $\gamma = 0.7$ seems to be a reasonable choice.

Finally, we plot the test accuracy against R the communication overhead for NASNetMobile in Fig. 16. In this figure, three schemes are considered, namely the proposed CO_3 with fp4, the proposed CO_3 with fp8, and the scheme that employs fp8 followed by the top_K . Here, the proposed scheme with fp4 and that with fp8 adopt the best $\gamma = 0.9$ and $\gamma = 0.7$ among those tested in Figs. 14 and 15, respectively. Moreover, for the top_K , we adopt $k = 0.5$. Each scheme is trained for 150 epochs, and the accuracy is tested based on the trained model. One observes in Fig. 16 that the proposed scheme is capable of achieving an accuracy that is comparable to or even better than the top_k while using a significantly less communication overhead.

VI. CONCLUSION

In this paper, we have investigated the problem of communication-efficient distributed DNN training. A novel framework, called CO_3 , has been proposed for the federated training of a centralized model. When specialized to DNN models, gradients are first quantized via floating-point conversion, lossless compressed by Huffman codes, and then corrected by adding the quantization error to the gradients in the next epoch. The effectiveness of CO_3 hinges on the fact that the distribution over the gradients can be well

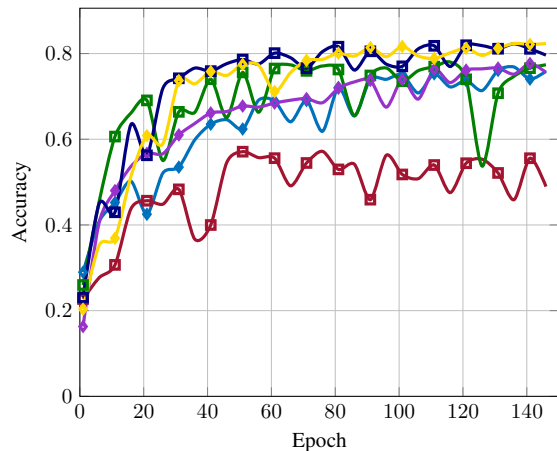


Fig. 13: Test accuracy of ResNet50V2. The communication overhead is $R_{fp4,Res} = 2.46 \times 10^{12}$ bits.

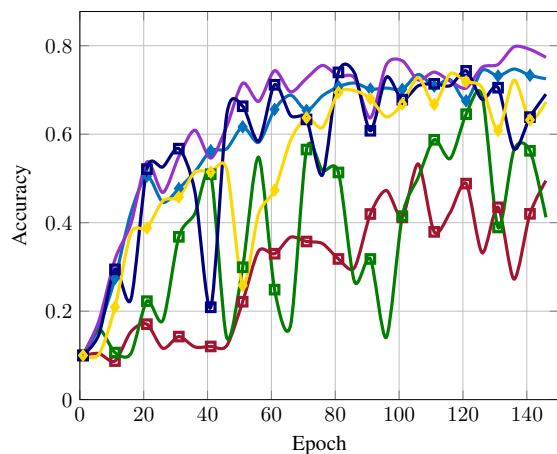


Fig. 14: Test accuracy of NASNetMobile. The communication overhead is $R_{fp4,NAS} = 3.43 \times 10^{11}$ bits.

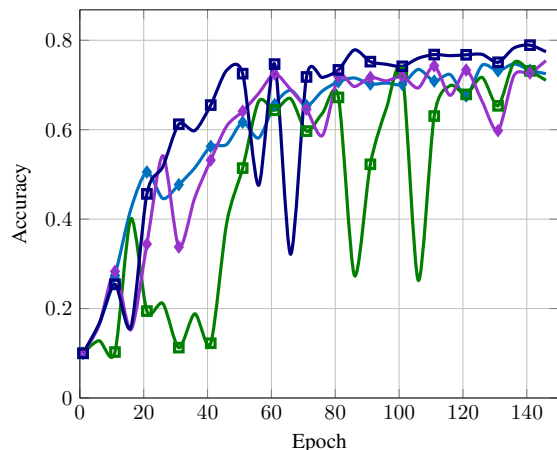


Fig. 15: Test accuracy of NASNetMobile. The communication overhead is $R_{fp8,NAS} = 3.65 \times 10^{11}$ bits.

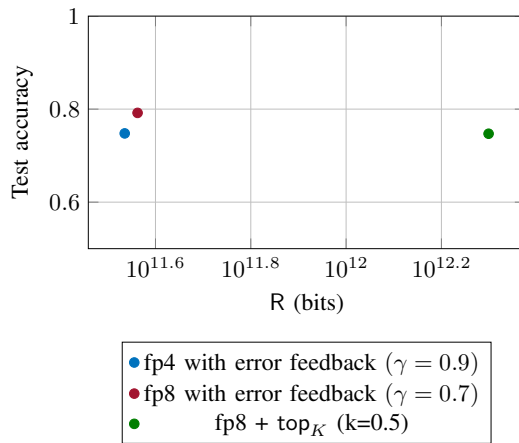


Fig. 16: The communication overhead versus test accuracy of different compression schemes of NASNetMobile.

defined. For the DNN case, we argue that the floating point conversions and Huffman coding can be efficiently designed by assuming that the gradient are i.i.d. distributed in each layer and are independent across layer and epochs (but with possibly different parameters). We refer to this assumption as the GenNorm assumption. In this paper, this assumption has been verified by a series of simulation, which has in turn allowed us to build a statistical model for gradients in DNN training. Extensive simulations have been conducted to demonstrate that CO₃ provide competitive DNN training performance at a significantly lower communication overhead. In particular, CO₃ is capable of achieving test accuracy performance that is comparable to the network trained with full SGD computation.

REFERENCES

- [1] J. Dean, G. Corrado, R. Monga, K. Chen, M. Devin, M. Mao, M. Ranzato, A. Senior, P. Tucker, K. Yang *et al.*, “Large scale distributed deep networks,” *Advances in neural information processing systems*, vol. 25, 2012.
- [2] T. Ben-Nun and T. Hoefler, “Demystifying parallel and distributed deep learning: An in-depth concurrency analysis,” *ACM Computing Surveys (CSUR)*, vol. 52, no. 4, pp. 1–43, 2019.
- [3] D. Bertsekas and J. Tsitsiklis, *Parallel and distributed computation: numerical methods*. Athena Scientific, 2015.
- [4] N. S. Shai Shalev-Shwartz and T. Zhang, “Trading accuracy for sparsity in optimization problems with sparsity constraints,” *SIAM J. Optimization*, 2010.
- [5] H. Wang, S. Sievert, S. Liu, Z. Charles, D. Papailiopoulos, and S. Wright, “Atomo: Communication-efficient learning via atomic sparsification,” in *Advances in Neural Information Processing Systems*, 2018, pp. 9850–9861.
- [6] D. Alistarh, T. Hoefler, M. Johansson, N. Konstantinov, S. Khirirat, and C. Renggli, “The convergence of sparsified gradient methods,” in *Advances in Neural Information Processing Systems*, 2018, pp. 5973–5983.
- [7] J. Bernstein, Y.-X. Wang, K. Azizzadenesheli, and A. Anandkumar, “signSGD: Compressed optimization for non-convex problems,” in *Advances in Neural Information Processing Systems*, 2018, pp. 560–569.
- [8] N. Agarwal, A. T. Suresh, F. X. Yu, S. Kumar, and B. McMahan, “cpSGD: Communication-efficient and differentially-private distributed SGD,” in *32nd Advances in Neural Information Processing Systems (NIPS)*, Montréal, Canada, Dec. 2018, pp. 7564–7575.
- [9] T. Li, Z. Liu, V. Sekar, and V. Smith, “Privacy for free: Communication efficient learning with differential privacy using sketches,” Available: <https://arxiv.org/abs/1911.00972>, 2019.
- [10] R. Saha, S. Rini, M. Rao, and A. Goldsmith, “Decentralized optimization over noisy, rate-constrained networks: Achieving consensus by communicating differences,” *IEEE J. Select. Areas Commun.*, 2021.
- [11] N. Shlezinger, S. Rini, and Y. C. Eldar, “The communication-aware clustered federated learning problem,” in *2020 IEEE International Symposium on Information Theory (ISIT)*. IEEE, 2020, pp. 2610–2615.
- [12] D. Alistarh, D. Grubic, J. Li, R. Tomioka, and M. Vojnovic, “Qsgd: Communication-efficient sgd via gradient quantization and encoding,” *Advances in Neural Information Processing Systems*, vol. 30, 2017.
- [13] J. Wangni, J. Wang, J. Liu, and T. Zhang, “Gradient sparsification for communication-efficient distributed optimization,” *Advances in Neural Information Processing Systems*, vol. 31, 2018.
- [14] V. Gandikota, R. K. Maity, and A. Mazumdar, “vqSGD: Vector quantized stochastic gradient descent,” *IEEE Trans. Inf. Theory*, 2022, to appear.
- [15] S. Salehkalaibar and S. Rini, “Lossy gradient compression: How much accuracy can one bit buy?” *arXiv preprint arXiv:2202.02812*, 2022.
- [16] F. Seide, H. Fu, J. Droppo, G. Li, and D. Yu, “1-bit stochastic gradient descent and its application to data-parallel distributed training of speech dnns,” in *INTERSPEECH*, 2014, pp. 9850–9861.
- [17] J. Konečný, H. B. McMahan, F. X. Yu, P. Richtárik, A. T. Suresh, and D. Bacon, “Federated learning: Strategies for improving communication efficiency,” Available: <https://arxiv.org/abs/1610.05492v1>, 2016.
- [18] X. Sun, J. Choi, C.-Y. Chen, N. Wang, S. Venkataramani, V. V. Srinivasan, X. Cui, W. Zhang, and K. Gopalakrishnan, “Hybrid 8-bit floating point (hfp8) training and inference for deep neural networks,” *Advances in Neural Information Processing Systems*, vol. 32, pp. 4900–4909, 2019.
- [19] Z.-J. Chen, E. E. Hernandez, Y.-C. Huang, and S. Rini, “DNN gradient lossless compression: Can GenNorm be the answer?” in *IEEE International Conference on Communications*, 2022.
- [20] S. P. Karimireddy, Q. Rebjock, S. Stich, and M. Jaggi, “Error feedback fixes signsgd and other gradient compression schemes,” in *International Conference on Machine Learning*. PMLR, 2019, pp. 3252–3261.
- [21] F. Seide, H. Fu, J. Droppo, G. Li, and D. Yu, “1-bit stochastic gradient descent and its application to data-parallel distributed training of speech dnns,” in *Fifteenth Annual Conference of the International Speech Communication Association*. Citeseer, 2014.
- [22] S. Bengio, H. Wallach, H. Larochelle, K. Grauman, N. Cesa-Bianchi, and R. Garnett, “Sparsified SGD with Memory,” *Advances in Neural Information Processing Systems*, vol. 31, 2018.
- [23] G. Huang, Z. Liu, L. Van Der Maaten, and K. Q. Weinberger, “Densely connected convolutional networks,” in *Proceedings of the IEEE conference on computer vision and pattern recognition*, 2017, pp. 4700–4708.
- [24] K. He, X. Zhang, S. Ren, and J. Sun, “Identity mappings in deep residual networks,” in *European conference on computer vision*. Springer, 2016, pp. 630–645.
- [25] B. Zoph, V. Vasudevan, J. Shlens, and Q. V. Le, “Learning transferable architectures for scalable image recognition,” in *Proceedings of the IEEE conference on computer vision and pattern recognition*, 2018, pp. 8697–8710.
- [26] S. Mei, A. Montanari, and P.-M. Nguyen, “A mean field view of the landscape of two-layer neural networks,” *Proceedings of the National Academy of Sciences*, vol. 115, no. 33, pp. E7665–E7671, 2018.
- [27] D. Araújo, R. I. Oliveira, and D. Yukimura, “A mean-field limit for certain deep neural networks,” *arXiv preprint arXiv:1906.00193*, 2019.
- [28] P.-M. Nguyen and H. T. Pham, “A rigorous framework for the mean field limit of multilayer neural networks,” *arXiv preprint arXiv:2001.11443*, 2020.
- [29] C. Fang, J. Lee, P. Yang, and T. Zhang, “Modeling from features: a mean-field framework for over-parameterized deep neural networks,” in *Conference on learning theory*. PMLR, 2021, pp. 1887–1936.
- [30] S. Mei, T. Misiakiewicz, and A. Montanari, “Mean-field theory of two-layers neural networks: dimension-free bounds and kernel limit,” in *Conference on Learning Theory*. PMLR, 2019, pp. 2388–2464.
- [31] J. Sirignano and K. Spiliopoulos, “Mean field analysis of neural networks: A law of large numbers,” *SIAM Journal on Applied Mathematics*, vol. 80, no. 2, pp. 725–752, 2020.
- [32] S. Shi, X. Chu, K. C. Cheung, and S. See, “Understanding top-k sparsification in distributed deep learning,” *arXiv preprint arXiv:1911.08772*, 2019.
- [33] J. Ziv and A. Lempel, “Compression of individual sequences via variable-rate coding,” *IEEE Trans. Inf. Theory*, vol. 24, no. 5, pp. 530–536, 1978.
- [34] I. Kontoyiannis, “Second-order analysis of lossless and lossy versions of lempel-ziv codes,” in *Conference Record of the Thirty-First Asilomar Conference on Signals, Systems and Computers (Cat. No. 97CB36136)*, vol. 2. IEEE, 1997, pp. 1349–1353.
- [35] T. M. Cover and J. A. Thomas, *Elements of Information Theory*, 2nd ed. New York, NY, USA: John Wiley & Sons, Inc., 2006.

- [36] B. Isik, A. No, and T. Weissman, "Successive pruning for model compression via rate distortion theory," *arXiv preprint arXiv:2102.08329*, 2021.
- [37] C. Villani, *Optimal Transport: Old and New*. Berlin Heidelberg: Springer, 2008.
- [38] S. U. Stich and S. P. Karimireddy, "The error-feedback framework: Better rates for sgd with delayed gradients and compressed communication," *arXiv preprint arXiv:1909.05350*, 2019.
- [39] A. Fraysse, B. Pesquet-Popescu, and J.-C. Pesquet, "Rate-distortion results for generalized Gaussian distributions," in *in Proc. IEEE International Conference on Acoustic, Speech, and Signal Processing*, Las Vegas, NV, USA, May 2008.